Fluorescence Spectroscopy for Real-Time Intraoperative Detection of Middle-Ear Cholesteatoma

Joackim Mahdjoub, Olivier Gaiffe, Riham Altaisan, Nikolaos Zirganos, Nicolas Passilly, Bruno Wacogne, Emmanuel Ramasso, Laurent Tavernier

Abstract:

Objective.
To evaluate whether autofluorescence spectroscopy (AFS) can reliably distinguish cholesteatoma from surrounding middle-ear tissues, and to develop a real-time intraoperative diagnostic tool.
Study Design. Prospective ex vivo study. Setting. Besançon University Hospital, France (tertiary care center).
Methods.
In this prospective ex vivo study, middle-ear tissue biopsies were collected during cholesteatoma surgeries and analyzed using autofluorescence following 405-nm laser excitation. Each sample was classified based on its spectral signature and confirmed by histopathology. A computer assisted model was applied to differentiate cholesteatoma from noncholesteatoma tissues, and its performance was assessed using standard cross-validation.
Results.
Thirty-six tissue samples from 23 patients were analyzed, generating nearly 3800 fluorescence spectra. The model correctly classified all samples, achieving 94.5% accuracy, 94.7% sensitivity, and 94.2% specificity. The system provided consistent performance across tissue types and returned results in real time, with a response time of 0.1 seconds per sample. Each output included a probability score indicating the likelihood of cholesteatoma presence.
Conclusion.
AFS demonstrated high accuracy in distinguishing cholesteatoma from other middle-ear tissues. Its speed, simplicity, and probabilistic feedback suggest strong potential for real-time intraoperative use. Once validated in vivo, this technology could assist surgeons by improving tissue discrimination and potentially reducing recurrence rates.

Introduction

Cholesteatoma is a progressive and destructive pathology of the middle ear, characterized by the accumulation of keratinizing squamous epithelium within the tympanic cavity or mastoid [1]. Although it often presents with relatively benign symptoms such as otorrhea and conductive hearing loss, it can lead to serious complications, including ossicular chain erosion, facial nerve palsy, labyrinthine fistula, and, in rare cases, intracranial infections.
Surgical excision remains the only curative treatment. However, achieving complete removal is often challenging due to the difficulty in distinguishing cholesteatoma from surrounding nonpathological structures during surgery. Residual or recurrent disease has been reported in 10% to 50% of cases [2,3]. Major factors contributing to residual disease are related to poor surgical visualization [4]. Several studies support the use of endoscopic devices during cholesteatoma surgery. However, even with the combined use of the endoscope and the operating microscope, complete disease eradication cannot always be achieved, although residual rates can be reduced by up to 50% [5]. This suggests that, despite good visualization of the middle-ear cavity, and even for experienced surgeons, small remnants of cholesteatoma matrix may remain indistinguishable from the underlying bone or mucosa. This underscores the clinical need for a real-time, objective, label-free intraoperative tool to improve tissue discrimination and ensure complete surgical excision.

In this context, several optical diagnostic modalities have been explored, including Raman spectroscopy [6] autofluorescence imaging [7-9] and multispectral imaging [10-12]. Some approaches rely on exogenous fluorescent agents, but these are constrained by safety concerns, regulatory limitations, and intraoperative workflow challenges [13, 14].
Autofluorescence spectroscopy (AFS) offers a compelling alternative as a rapid, label-free method for tissue characterization in both head and neck oncology and otologic surgery [10, 15-19]. Previous research has demonstrated that 405-nm excitation enables differentiation between keratinized and non-keratinized tissue and allows assessment of metabolic activity through optical redox ratios—features particularly relevant to cholesteatoma identification [7, 20]. A recent study [21] showed that rigid endoscopic autofluorescence imaging excited at 405 nm can effectively differentiate the cholesteatoma matrix and keratin from the surrounding mucosa.
The optical system developed for this study utilizes a fiber-optic probe to enable localized tissue assessment, delivering immediate, real-time data in a compact, portable configuration optimized for intraoperative surgical application. As part of ongoing research into assisted and semi-autonomous surgical workflows, this system is being tested for compatibility with robotic platforms.
The objective of this study was to assess the diagnostic accuracy of AFS combined with a machine learning model in distinguishing cholesteatoma from adjacent middle-ear tissues in an ex vivo setting. This work lays the foundation for future in vivo validation and potential clinical application during middle-ear surgery.

Materials and Methods

Study design and subjects

This prospective ex vivo study was conducted between 2021 and 2022. It was deemed to fall outside the scope of the Jardé Law and does not meet the definition of research involving human participants as specified in Article L1122-1 of the French Public Health Code. As such, approval from an ethics committee was not required.
The study was registered by the University Hospital of Besançon (CHU de Besançon). Data collection and processing were carried out by a team from the CHU de Besançon in compliance with the European General Data Protection Regulation (GDPR) and in accordance with the guidelines of the French Data Protection Authority (CNIL). All patient data were fully anonymized before analysis.
Middle ear biopsies were collected during routine cholesteatoma surgeries, immediately placed in a saline solution, and analyzed using autofluorescence spectral acquisition before being sent for histopathological confirmation.

Fluorescence spectroscopic measurements

Autofluorescence spectral measurements were performed using a custom-designed spectroscopy system combining a 405-nm laser source with a fiber-optic probe for localized tissue interrogation [22]. The fiber-optic probe used in this study was designed as a modular interface, adaptable for either manual use or integration with a robotic surgical platform. This dual-use configuration enables flexible deployment of the system in both conventional and robot-assisted surgical settings.
Spectral data were acquired over a 2 mm × 2 mm tissue area with a spatial resolution of 200 µm, enabling hyperspectral mapping of the tissue surface. To maintain spatial correspondence between acquisition points and tissue architecture, the system incorporated a position-calibrated imaging module (figure1A). Acquired images were processed with a segmentation algorithm to exclude pixels located outside the tissue boundaries, thereby improving the accuracy and relevance of the spectral analysis (figure 1B).

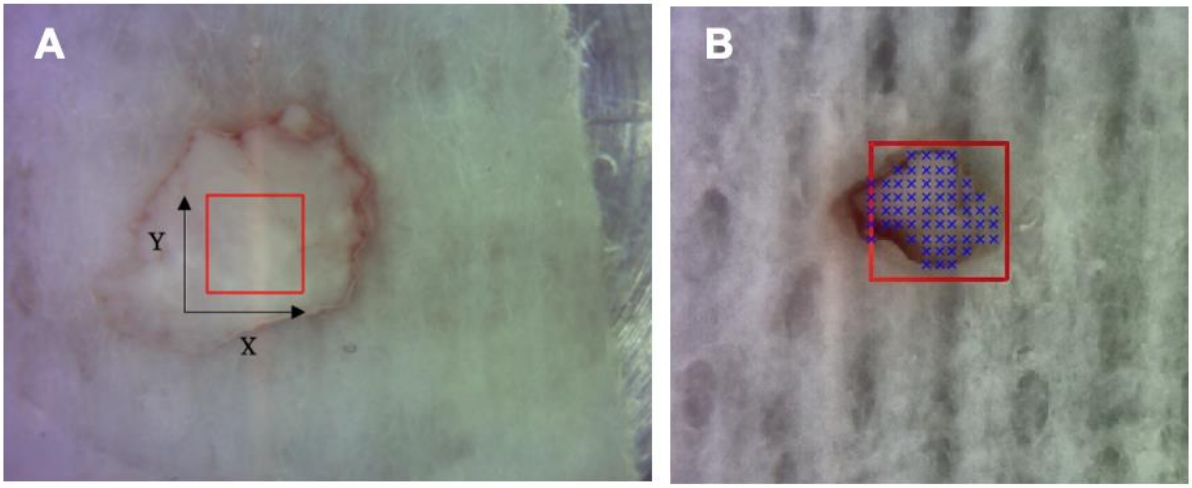

Figure 1: (A) Image of the 4 mm² scan (red square) on a cholesteatoma matrix sample; (B) Segmentation process applied to the calibrated image of a sample, designed to remove data points located outside the sample.

Fluorescence spectra were normalized using the area-under-the-curve (nAUC) to minimize the effects of excitation intensity and reflectivity variation across samples. Spectra exhibiting signal saturation or a signal-to-noise ratio <20 dB were excluded from analysis.

Data analysis and classification

Fluorescence spectra of biological tissues typically comprise hundreds of closely spaced wavelength measurements, many of which are highly correlated and therefore partially redundant. To address this, we applied Principal Component Analysis (PCA), a statistical technique commonly used for dimensionality reduction and pattern identification in spectral data. PCA transforms the original correlated variables into a smaller set of uncorrelated variables, called principal components (PCs). Each PC represents a distinct pattern of spectral variation and combines the contribution of multiple wavelengths into a single axis of variation. This transformation enhances interpretability and facilitates the identification of meaningful differences between tissue types.
A component selection strategy referred to as “PCA Sequential Forward Selection” (PCA-SFS) approach was implemented [23] which involved the progressive inclusion of PCs only when they improved diagnostic accuracy (Acc). This method enhanced classification performance by improving class separation and reducing the risk of overfitting. The selected components were used as input for a Quadratic Discriminant Analysis (QDA) model to classify each spectrum as either “cholesteatoma” or “non-cholesteatoma middle-ear tissues”.
A 5-fold cross-validation method was implemented to assess model robustness.
For each biopsy, which includes multiple spectral measurements, the final classification was determined by the class (cholesteatoma or noncholesteatoma) most frequently predicted among all spectra from that sample. Diagnostic accuracy, sensitivity, and specificity were calculated, each reported with 95% confidence intervals (CIs). All analyses were performed using MATLAB R2023a (The MathWorks Inc.).

Results

Population and sample characteristics

A total of 23 patients (13 males, 10 females; mean age: 38 years, range: 12-79 years) were included in the study. From these patients, 36 middle-ear tissue samples were collected. Histopathological

examination classified the samples into 8 distinct categories: cholesteatoma (matrix), cholesteatoma (keratin debris), mucosa, bone, cartilage, connective tissue, muscle, and tympanosclerosis. After preprocessing and quality control, 3787 fluorescence spectra were retained for analysis. Table 1 details the distribution of samples and selected spectra across tissue types.

Table 1. Distribution of selected spectra

Histologic class	Number of spectra recorded[1]		Number of samples[1]	
All biopsies	**3,787**	**(100)**	**38**	**(100)**
Cholesteatoma	**1,953**	**(51.6)**	**17**	**(44.7)**
Cholesteatoma (keratin debris)	1,007	(26.6)	9	(23.7)
Cholesteatoma (matrix)	946	(25.0)	8	(21.1)
Other	**1,834**	**(48.4)**	**21**	**(55.3)**
Bone	399	(10.5)	4	(10.5)
Cartilage	484	(12.8)	4	(10.5)
Connective tissue	535	(14.1)	6	(15.8)
Mucosa	123	(3.2)	4	(10.5)
Muscle	230	(6.1)	2	(5.3)
Tympanosclerosis	63	(1.7)	1	(2.6)

[1]: n (%)

Classification: cholesteatoma versus other tissues

The classification model using the PCA-SFS and QDA approach achieved an overall accuracy of 94.5%, with a sensitivity of 94.7% (95% CI: 93.6%-95.7%) and a specificity of 94.2% (95% CI: 93.1%-95.2%). As illustrated in figure 2, the classification accuracy increased rapidly with the inclusion of the first few PCs, reaching over 93% with just 6 components. The highest accuracy (94.38%) was observed when using 11 components.

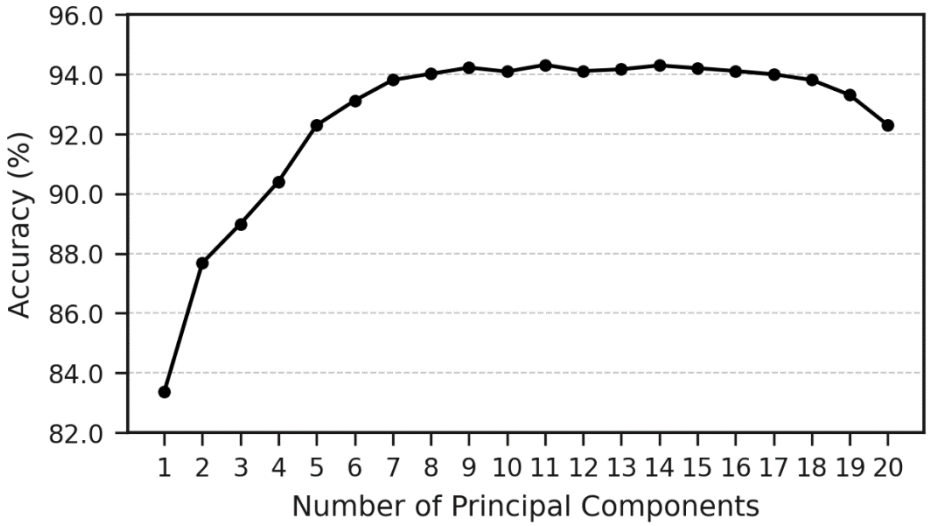

Figure 2: Classification accuracy (%) obtained using a quadratic discriminant analysis (QDA) model as a function of the number of principal components (PCs). The PCs were selected based on their contribution to improving classification performance (PCA-SFS).

Classification accuracy (%) obtained using a quadratic discriminant analysis (QDA) model as a function of the number of principal components (PCs). The PCs were selected based on their contribution to improving classification performance (PCA-SFS).
Beyond this point, the performance began to decline slightly or plateau, suggesting that adding more components does not necessarily lead to better classification and may introduce redundancy or noise. Overall, the PCA-SFS approach enabled the model to achieve high accuracy with fewer components, demonstrating the advantage of targeted component selection over traditional variance-based ordering.
All samples were correctly classified as either cholesteatoma or noncholesteatoma. These results emphasize that selecting PCs based on their contribution to classification performance yields a more accurate and robust model than relying on explained variance alone.

Discussion

This study presents the first report of a classification technique for middle-ear cholesteatoma based on AFS combined with machine learning. Our model achieved a high diagnostic performance, with an accuracy of 94.5%, demonstrating its potential for real-time intraoperative tissue discrimination.
Cholesteatoma surgery is often complicated by the risk of residual disease, mainly due to limited intraoperative visualization. The use of white-light endoscopy helps reduce this risk by improving the surgeon's view of hidden areas. However, it has proven insufficient to completely eradicate residual cholesteatomas. This indicates that distinguishing pathological tissue from adjacent normal structures remains challenging. In this context, a rapid, reliable, and objective tool to assist in intraoperative identification is critically needed. Our findings support the potential of AFS to address this clinical gap.
As reported by Le Nobel et al [24], impaired surgical field clarity due to intraoperative bleeding is also associated with an increased risk of residual cholesteatoma. This is particularly relevant in endoscopic ear surgery, where the management of bleeding is more challenging. Bleeding generally causes a lack of fluorescence intensity. However, our novel method combining AFS and a thorough data processing enables cholesteatoma identification independently of fluorescence intensity. Moreover, our device has been designed for intraoperative endoscopic use, making it suitable for visualizing anatomically difficult regions such as the sinus tympani or the facial recess.
Previous optical approaches have explored otoscopic autofluorescence, Raman spectroscopy, and deep learning on otoscopic images. However, most of these studies involved small sample sizes or lacked quantitative validation. For instance, Valdez et al [8, 9] evaluated autofluorescence-based tools in pediatric populations and ex vivo tissues, respectively, but included no more than 11 tissue samples and did not report diagnostic performance metrics.
Other groups have focused on using optical image-based classification methods, often involving deep learning. Cavalcanti et al [25] trained several classifiers using a smartphone modified for autofluorescence imaging to distinguish normal tympanic membranes from chronic otitis media but obtained only moderate accuracies (50%-79%). Tseng et al [26] applied convolutional neural networks (CNNs) to otoscopic images and reported high specificity (96.5%) but only moderate sensitivity (63.6%), which limits their usefulness in reliably detecting disease. Although these otoscopy-based methods may support the early-stage detection of middle ear pathology, they remain unsuitable for the intraoperative identification of residual disease, which requires real-time and high-precision tools.
Few studies have attempted to evaluate intraoperative optical discrimination. In a proof-of-concept study, Wisotzky et al [27] combined multispectral imaging with white-light endoscopy in 3 patients, showing promising but nonquantified results. More recently, Miwa et al [28] tested CNNs on intraoperative endoscopic images but reported limited performance, with a sensitivity of 42.3% and specificity of 87.5%.
In contrast, our AFS-based method was designed from the outset with intraoperative application in mind. It combines rapid acquisition, robust spectral processing, and a simple classification model

(QDA), enabling potential real-time integration into surgical workflows. This approach represents a significant advancement over previous studies, offering higher performance and clinical relevance.

While the diagnostic results are promising, several limitations must be acknowledged. First, the study was conducted in an ex vivo setting, which does not fully replicate the optical and physiological conditions encountered during surgery, such as tissue perfusion, temperature, and motion. As such, in vivo validation will be necessary to confirm the feasibility and clinical utility of the technique in the operative environment.

Blood strongly absorbs excitation light around 405 nm due to hemoglobin, which can reduce the measured fluorescence signal. In the present study, fluorescence spectra were nAUC, making the classification largely independent of signal amplitude. However, blood absorption may also induce characteristic distortions in spectral shape, particularly in wavelength regions associated with hemoglobin absorption bands. In such situations, these alterations are treated as signal perturbations, prompting operator notification and suspension of classification until adequate signal conditions are restored. Despite these precautions, in vivo translation will introduce additional challenges related to tissue vascularization, motion artifacts, and acquisition stability.

Second, although 36 tissue samples were analyzed, the number of patients per tissue category remains limited, which may affect the generalizability of the model. Nevertheless, the statistical strength of the analysis primarily arises from the large number of independent spectra acquired at each measurement site (1953 for cholesteatoma and 1834 for noncholesteatoma tissues). Each spectrum corresponds to a distinct optical measurement, providing a rich dataset that enables robust machine-learning validation despite the relatively small number of biopsy samples. However, expanding the dataset in future multicenter studies would improve model robustness and allow for the inclusion of additional critical anatomical structures, such as the facial nerve or dura mater, which were not represented here for ethical reasons.

Although we used QDA for its simplicity and clinical compatibility, future studies could explore more complex classification algorithms, such as support vector machines or deep learning models, which may offer improved performance, especially in more heterogeneous datasets.

In summary, this study demonstrates the feasibility of using AFS combined with machine learning for the differentiation of cholesteatoma from noncholesteatoma middle-ear tissues. For future in vivo applications, this approach could be translated either through the direct use of a similar rigid probe or by adapting the system to a flexible optical fiber device, which would facilitate the exploration of the middle-ear cavity. A probe prototype has been specifically designed to be compatible with a robotic system for ear surgery, allowing precise and stable manipulation during minimally invasive procedures. Alternatively, the spectral bands identified with the PCA in our study could be exploited for the development of real-time autofluorescence hyperspectral imaging, enabling intraoperative visualization of suspected cholesteatoma areas. With further validation, this approach could support real-time intraoperative guidance, improve surgical precision, and reduce recurrence rates. These findings provide a strong foundation for future in vivo clinical studies and the development of integrated AFS-based surgical tools.

Conclusion

This study provides the first evidence to support the use of AFS for cholesteatoma classification, achieving an accuracy of 94.5% on ex vivo samples. The normalization of fluorescence spectra, by correcting for variations in absorption and excitation intensity, contributes to the design of a robust system, ensuring stable diagnostic performance across different samples and acquisition conditions. The real-time applicability suggests a potential for intraoperative use to improve surgical precision and reduce recurrence rates. Future in vivo validation will be essential to confirm its clinical impact.

References

1. Yung M, Tono T, Olszewska E, et al. EAONO/JOS joint consensus statements on the Definitions, Classification and Staging of Middle Ear Cholesteatoma. *Journal of International Advanced Otology*. *Mediterranean Society of Otology and Audiology*. 2017;13(1):1-8. doi:10.5152/iao.2017.3363
2. Aquino JEAP de, Cruz Filho NA, Aquino JNP de. Epidemiology of middle ear and mastoid cholesteatomas: study of 1146 cases. *Braz J Otorhinolaryngol*. 2011;77(3):341-347. doi:10.1590/S1808-86942011000300012
3. Sheehy JL, Brackmann DE, Graham MD. Cholesteatoma Surgery: Residual and Recurrent Disease: A Review Of 1,024 Cases. *Annals of Otology, Rhinology & Laryngology*. 1977;86(4):451-462. doi:10.1177/000348947708600405
4. Volgger V, Lindeskog G, Krause E, Schrötzlmair F. Identification of risk factors for residual cholesteatoma in children and adults: a retrospective study on 110 cases of revision surgery. *Braz J Otorhinolaryngol*. 2020;86(2):201-208. doi:10.1016/j.bjorl.2018.11.004
5. Kozin ED, Gulati S, Kaplan AB, et al. Systematic review of outcomes following observational and operative endoscopic middle ear surgery. *Laryngoscope*. 2015;125(5):1205-1214. Doi:10.1002/lary.25048
6. Pandey R, Paidi SK, Kang JW, et al. Discerning the differential molecular pathology of proliferative middle ear lesions using Raman spectroscopy. *Sci Rep*. 2015;5:13305. doi:10.1038/srep13305
7. Yang S, Farrell J, Ye S, Ahmad I, Valdez TA. Imaging guidance for cholesteatoma surgery using tissue autofluorescence. *J Biomed Opt*. 2023;28(06). doi:10.1117/1.JBO.28.6.066003
8. Valdez TA, Pandey R, Spegazzini N, Barman I, Dasari RR. A smarter view of the ear with chemical imaging. *SPIE Newsroom*. Published online November 30, 2015. doi:10.1117/2.1201510.006193
9. Valdez TA, Pandey R, Spegazzini N, et al. Multiwavelength Fluorescence Otoscope for Video-Rate Chemical Imaging of Middle Ear Pathology. *Anal Chem*. 2014;86(20):10454-10460. doi:10.1021/ac5030232
10. Zhou Z, Pandey R, Valdez TA. Label-Free Optical Technologies for Middle-Ear Diseases. *Bioengineering*. 2024;11(2):104. doi:10.3390/bioengineering11020104
11. Wisotzky EL, Rosenthal JC, Hilsmann A, Eisert P, Uecker FC. A multispectral 3D-Endoscope for Cholesteatoma Removal. In: *Current Directions in Biomedical Engineering*. Vol 6. Walter de Gruyter GmbH; 2020. doi:10.1515/cdbme-2020-3065
12. Valdez TA, Spegazzini N, Pandey R, et al. Multi-color reflectance imaging of middle ear pathology in vivo. *Anal Bioanal Chem*. 2015;407(12):3277-3283. doi:10.1007/s00216-015-8580-y
13. Levy LL, Jiang N, Smouha E, Richards-Kortum R, Sikora AG. Optical imaging with a high-resolution microendoscope to identify cholesteatoma of the middle ear. *Laryngoscope*. 2013;123(4):1016-1020. doi:10.1002/lary.23710

14. Early S, Saad MA, Mallidi S, et al. A fluorescent photoimmunoconjugate for imaging of cholesteatoma. *Sci Rep*. 2022;12(1):19905. doi:10.1038/s41598-022-22072-9

15. Wu C, Gleysteen J, Teraphongphom NT, Li Y, Rosenthal E. In-vivo optical imaging in head and neck oncology: basic principles, clinical applications and future directions. *Int J Oral Sci*. 2018;10(2):10. doi:10.1038/s41368-018-0011-4

16. Francisco ALN, Correr WR, Pinto CAL, et al. Analysis of surgical margins in oral cancer using in situ fluorescence spectroscopy. *Oral Oncol*. 2014;50(6):593-599. doi:10.1016/j.oraloncology.2014.02.008

17. Gillenwater A, Jacob R, Ganeshappa R, et al. Noninvasive Diagnosis of Oral Neoplasia Based on Fluorescence Spectroscopy and Native Tissue Autofluorescence. *Arch Otolaryngol Head Neck Surg*. 1998;124(11):1251. doi:10.1001/archotol.124.11.1251

18. Nayak GS, Kamath S, Pai KM, et al. Principal component analysis and artificial neural network analysis of oral tissue fluorescence spectra: Classification of normal premalignant and malignant pathological conditions. *Biopolymers*. 2006;82(2):152-166. doi:10.1002/bip.20473

19. Jayanthi JL, Mallia RJ, Shiny ST, et al. Discriminant analysis of autofluorescence spectra for classification of oral lesions in vivo. *Lasers Surg Med*. 2009;41(5):345-352. doi:10.1002/lsm.20771

20. Chance B, Schoener B, Oshino R, Itshak F, Nakase Y. Oxidation-reduction ratio studies of mitochondria in freeze-trapped samples. NADH and flavoprotein fluorescence signals. *Journal of Biological Chemistry*. 1979;254(11):4764-4771. doi:10.1016/s0021-9258(17)30079-0

21. van der Toom HFE, de Bruijn HS, Pauw RJ, et al. Rigid Autofluorescence Imaging as a Tool for Identifying Cholesteatoma During Otologic Surgery: Initial Ex Vivo Findings. *Otolaryngology–Head and Neck Surgery*. 2025;173(2):461-467. doi:10.1002/ohn.1274

22. Gaiffe O, Mahdjoub J, Ramasso E, et al. Discrimination of vocal folds lesions by multiclass classification using autofluorescence spectroscopy: An ex vivo study. *Head Neck*. 2024;46(5):1136-1145. doi:10.1002/hed.27668

23. Jolliffe IT. *Principal Component Analysis*. Second Edi. Springer-Verlag; 2002. doi:10.1007/b98835

24. le Nobel GJ, Cushing SL, Papsin BC, James AL. Intraoperative Bleeding and the Risk of Residual Cholesteatoma: A Multivariate Analysis. *Otology & Neurotology*. 2017;38(4):529-534. doi:10.1097/MAO.0000000000001355

25. Cavalcanti TC, Lew HM, Lee K, Lee SY, Park MK, Hwang JY. Intelligent smartphone-based multimode imaging otoscope for the mobile diagnosis of otitis media. *Biomed Opt Express*. 2021;12(12):7765. doi:10.1364/boe.441590

26. Tseng CC, Lim V, Jyung RW. Use of artificial intelligence for the diagnosis of cholesteatoma. *Laryngoscope Investig Otolaryngol*. 2023;8(1):201-211. doi:10.1002/lio2.1008

27. Wisotzky EL, Rosenthal JC, Wege U, Hilsmann A, Eisert P, Uecker FC. Surgical Guidance for Removal of Cholesteatoma Using a Multispectral 3D-Endoscope. *Sensors*. 2020;20(18):5334. doi:10.3390/s20185334

28. Miwa T, Minoda R, Yamaguchi T, et al. Application of artificial intelligence using a convolutional neural network for detecting cholesteatoma in endoscopic enhanced images. *Auris Nasus Larynx*. 2022;49(1):11-17. doi:10.1016/j.anl.2021.03.018